AIAA JOURNAL
Vol. 37, No. 10, October 1999

Probabilistic Method for Predicting the Variability in Fatigue Behavior of 7075-T6 Aluminum

K. M. Gruenberg,* B. A. Craig,† and B. M. Hillberry‡
Purdue University, West Lafayette, Indiana 47907-1288

The applicability of a probabilistic model for estimating fatigue life variability for 7075-T6 aluminum is assessed. The test specimens for the experimental program were 7075-T6 aluminum single-edge notch-tension specimens tested under constant-amplitude loading (σ_{max} = 120 MPa, R = 0.01). A plastic replication procedure was used to identify crack nucleation sites and monitor crack growth. The initiation sites were identified by examination of the plastic replicas and the fracture surfaces of the failed specimens. In agreement with previous studies, the fatigue cracks formed in the center of the notch from material inclusions. For the prediction model, the distribution of inclusion sizes (0.2–45 μm^2) within the material were used as the distribution of initial flaw sizes. It was assumed that the crack formation life was a small percentage of the total life, and thus life predictions were based entirely on crack propagation. The cumulative distributions for the fatigue lives from the experimental work and the numerical model were compared to assess the effectiveness of the model. Whereas experimental crack formation lives as long as 50–70% of the total life were observed in some of the tests, the model predicted failures well in the shorter life regime. The predicted lives were conservative, and in the shortest life region the predictions were within 15% of the observed lives.

Introduction

ONE method that has been developed to address the variability in fatigue lives is a probabilistic approach.[1] This approach has been developed mainly from two observations in fatigue. First, fatigue studies have shown wide ranges of lifetimes within a given set of identical tests. Second, it has been observed that many fatigue failures have initiated at material inhomogeneities.[2] Taking into account the inherent microstructural variability and other fatigue analysis concepts, like stress-intensity factors, crack closure, and small-crack effects, a method has been constructed to estimate the variability in fatigue life to failure.[1] In addition, the method estimates this variability with reduced amounts of costly and time-consuming experimentation.

In the past two decades, fatigue crack growth behavior in the region of low-stress-intensity range ΔK has been closely examined. One result has been the concept that for any crack configuration for which the calculated ΔK is below a threshold level (ΔK_{th}) the crack will not propagate.[3–5]

It has been observed that cracks initiate very early in the fatigue life, occurring at a variety of material inhomogeneities,[2,6–8] such as voids, particles, or pits. For sheet materials, most of the porosity is eliminated during the rolling process. As a result, for a smooth surface of sheet material, the largest remaining defects are material inclusions.[9–11]

Previous studies have shown that the fatigue behavior of many materials depends heavily on the microstructure.[5,6,10,12–14] These studies discuss the roles of material inclusions, material phases, grain orientation, and other microstructural characteristics that influence crack growth. It has been observed that all of these features provide more pronounced effects when the crack is small.

Cracks have been observed to propagate such that the crack surfaces are perpendicular to the loading direction. It has also been observed[10,15] that fatigue cracks quickly assume a semicircular shape, $a/c = 1$. This, coupled with the preceding discussion about the different modes of crack initiation, can be used to develop a fatigue life prediction methodology that is based entirely on crack propagation.

Small cracks have been observed to grow faster than long cracks. Plasticity-induced closure reduces crack growth rates; however, small cracks have not developed any prior plastic deformation. The absence of closure effects for newly initiated cracks helped explain why low-stress-ratio loadings and compressive loadings resulted in faster crack growth rates than were predicted from long-crack data.[16] It has also been observed that cracks with different lengths, but the same ΔK, behaved differently.[4,10,11] The large difference between growth rates was attributed to crack length in which the observed growth rates were much faster than those predicted from the available da/dN vs ΔK relationships.[2,4,9,10,14,16]

Various investigations[2,14,15] have shown that there is an inherent nature about fatigue that produces varying fatigue lives for seemingly identical test configurations. Recently, investigators have made attempts to predict the variation in fatigue results.[1,11,13] In the study of Laz and Hillberry[1] of 2024-T3 aluminum sheet, a probabilistic method was developed to predict the variability in fatigue lives based on microstructural variability. The probabilistic model was found to provide a good prediction of the experimental fatigue lives and their associated variability.

The analysis of Laz and Hillberry implemented a Monte Carlo simulation to make analytical predictions of variability. The analysis used FASTRAN II,[17] a numerical crack growth model. This computer program, developed by Newman, incorporates the above-discussed theories of closure, small-crack effects, and da/dN vs ΔK_{eff} relations. In the FASTRAN II model, ΔK_{eff} is applied throughout the analysis, and the corresponding growth increment is calculated. In this study, as well as in the study of Laz and Hillberry, FASTRAN II was used to grow the cracks numerically to breakthrough.

Materials and Methods

Aluminum 7075-T6 Sheet

The material used in this study was an aluminum Al–Zn–Mg alloy 7075-T6 in the form of a 2.31-mm-thick sheet. This previously untested panel was from the same material lot as that tested by Edwards and Newman[18] and was provided by NASA Langley Research Center. The da/dN vs ΔK_{eff} data were developed by Newman et al.[2] for this material, and therefore no measurements of crack growth rates were performed.

Large constituent particles of the order of 2–50 μm in size are formed during the processing of the sheet material. These particles

Presented as Paper 98-2055 at the AIAA/ASME/ASCE/AHS/ASC 39th Structures, Structural Dynamics, and Materials Conference, Long Beach, CA, 20–23 April 1998; received 26 June 1998; revision received 1 February 1999; accepted for publication 26 February 1999.

*Graduate Research Assistant, School of Mechanical Engineering.
†Assistant Professor, Department of Statistics.
‡Professor, School of Mechanical Engineering. Member AIAA.

Table 1 Mechanical properties of 7075-T6[2,19]

Property	Value
$S_{Y0.2\%}$, MPa	503
S_u, MPa	572
K_c, MPa m$^{1/2}$	50

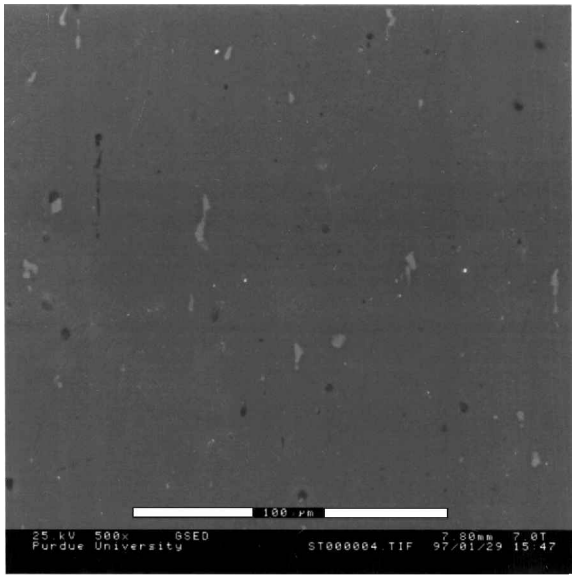

Fig. 1 Environmental scanning electron microscope image of ST plane at 500 ×.

are detrimental to the fatigue resistance of the alloy and actually act as fatigue crack formation sites.[19]

Figure 1 shows the appearance of these larger particles on the short-transverse (ST) plane of the 7075-T6 used in this study. The types of particles and precipitates formed in this alloy have nominal chemical compositions of $MgZn_2$, $Mg_3Zn_3Al_2$, Mg_2Si, Al_7Cu_2Fe, and Mg_5Al_3. Table 1 gives the mechanical properties of the 7075-T6 alloy.[20]

Experimental Testing

Test Specimens

Laz and Hillberry,[1] Newman et al.,[2] Newman and Edwards,[15] and Edwards and Newman[18] used a single-edge notch-tension (SENT) specimen to investigate the initiation and the growth behavior of small cracks. This specimen design was initially chosen because it simulated the behavior of an open hole in an aircraft structure.[15] This specimen geometry was used for the experimental component of this investigation. The dimensions for the specimens are based on previous studies[1,2,15]: length, 216 mm; width, 45 mm; thickness, 2.235 mm; and notch radius, 2.92 mm. The single notch was used to localize the region within which cracks would initiate. Figure 2 shows the orientation of the metallurgical planes and the loading direction with respect to the specimen. Also shown in the figure is the orientation of the crack that forms in this type of specimen. Laz and Hillberry[1] and Murakami and Endo[21] observed that the ST plane is the most relevant plane for nucleation sites in this type of configuration and loading.

Specimen Preparation

A total of 18 specimens was cut from one panel. To minimize the residual stresses, a series of 12 decreasing depths of cut were used to machine the notch, followed by a chemical polishing procedure. The chemical polishing process[2] removed a uniform, thin layer of material from the specimen, approximately 40 μm from each surface. The polishing procedure removed any remaining scratches and helped reduce any remaining residual stresses. The testing dimensions were chosen such that the ΔK solution, as developed by Newman et al., would be applicable.[2]

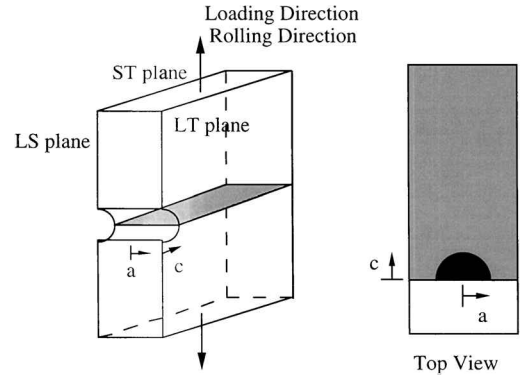

Fig. 2 SENT geometry and orientation of metallurgical plan: LS, longitudinal-short; LT, longitudinal-transverse.

Test Conditions

The tests were run in laboratory air with a 10-Hz, constant-amplitude sine wave. The maximum nominal stress applied was 120 MPa and the minimum stress was 1.2 MPa, so that the tests were run at a stress ratio R of 0.01. The load cycle was paused after predetermined cycle increments so that a replication procedure could be performed. To replicate the notch surface, we stopped the load cycling at the mean load and the load was raised to 80% of the maximum load. A drop of high-purity acetone was applied to the notch surface, and the acetyl cellulose film was lightly pressed into the notch. The acetone was allowed to set for a period of 5 min before the replica was removed. Replicas were examined with a light microscope at approximately 220× magnification for the presence of cracks in the notch. With this magnification, 20–40-μm cracks were readily detected, although at this resolution 5–6-μm cracks can be identified. For each test, the cycles to form a through-thickness crack (breakthrough) N_b and the cycles to failure N_f were recorded.

The purpose of the replicas was to provide a microscopic record of the notch surface throughout testing as well as to monitor crack growth. Each replica was stored so it could be examined in greater detail after testing. The replicas were examined in reverse order to help find the crack formation life N_i and the location and nature of the crack nucleation site.

Determination of ΔK_{th}

A value for ΔK_{th} was calculated from the experimental fatigue lives. FASTRAN II, which used the longest, finite experimental life, was used to determine the initial crack size A_i corresponding to the threshold. However, there is still a possibility of observing a longer lifetime than those observed in this investigation. To address this possibility, the cumulative distribution value associated with the longest observed lifetime was taken to be the cumulative distribution value of the corresponding initial crack size A_i. The threshold crack size A_{th} was determined by finding the appropriate crack size that matched the cumulative percentage based on the area distribution to the observed cumulative percentage for the longest, finite lifetime. The threshold area is used as a lower bound for initial areas in the probabilistic model, which will be discussed below. The assumption is that any initial crack with an area below the threshold value will not propagate.

Probabilistic Modeling

Based on the observations and theories from the literature, several assumptions are incorporated into the probabilistic model:

1) Cracks form at particles at the center of the notch (0 deg from the ST plane).

2) Crack formation occurs in the middle of the specimen thickness.

3) Cracks form as surface cracks and assume a semicircular shape in the ST plane.

4) A nucleating defect is assumed to be a flat crack.

5) The crack propagation path is parallel to the ST plane.

6) Formation life is a small percentage of the total life and can be neglected.

For the probabilistic model, particle areas were measured and fitted to a three-parameter log-normal distribution. The distribution

was then used for two separate failure predictions. The first prediction used a Monte Carlo simulation to sample, from the estimated distribution of particle areas, 1000 particle sizes greater than the threshold area. The projected area A_i of the initiating defect was converted to a semicircular crack of radius r_i. These generated cracks were numerically grown to failure by use of FASTRAN II. The second prediction used conditional probability to create a cumulative distribution for particle size and then took advantage of the one-to-one relation between particle area A_i and life to breakthrough N_b to compile a cumulative distribution function (CDF) for fatigue lives. The Monte Carlo procedure, implemented in earlier work by Laz and Hillberry,[1] produces an estimate of the exact CDF. The conditional probability procedure is an improvement since it produces the exact CDF. Both procedures are used here to verify previous results.

Area Distribution Analysis

For particle analysis, two small coupons of sheet material were cut from the same panel as the test specimens. The coupons were mounted on Bakelite, and the ST surface was polished with 100-, 320-, 400-, and 600-grit rotating sanding wheels. Two wet polishes, a 5-μm diamond paste and a 0.05-μm CrO_3 slurry, were used to achieve the final surface finish.

To document the particle area distribution, we photographed the mounted coupons with an environmental scanning electron microscope (ESEM). Twenty pictures of the ST plane were taken at a magnification of 500×. One such image is shown in Fig. 1. The pictures were taken across the entire exposed area of the coupons so as to take a representative sample of the particle distribution. The particles in the ST plane, perpendicular to the loading direction, are the particles relevant to the initiating crack shapes.[1,21]

An image analysis package, IMIX,[22] was used to measure the area of each particle. Figure 3 shows the binary image corresponding to Fig. 1. After calibration, the program converted the white pixels into particle areas. The image analysis resulted in the measurement of 1282 particles from the total area examined, which was a little more than 0.5 mm^2. With this set of equipment, a particle of 0.05 μm^2 could be resolved, although the smallest observed particle was 0.2 μm^2.

As in the analysis of Laz and Hillberry of 2024-T3, a three-parameter log-normal distribution was fit to the distribution of particle areas. Equation (1) shows the general form of the density function of a three-parameter log-normal distribution:

$$f(A) = \frac{1}{\sqrt{2\pi}(A-\theta)\sigma} \exp\left\{-\frac{1}{2}\left[\frac{\ell n(A-\theta)-\zeta}{\sigma}\right]^2\right\} \qquad (1)$$

where θ, σ, and ζ represent the threshold, shape, and scale parameters, respectively. To fit these parameters to the measured data, a

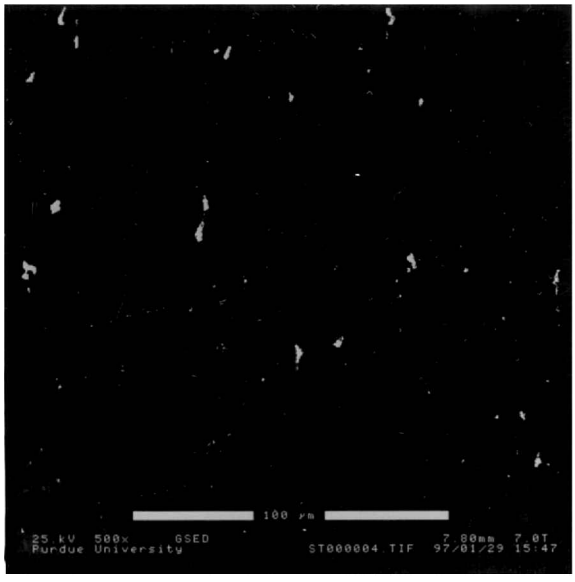

Fig. 3 Black-and-white image (of Fig. 1) used in particle analysis.

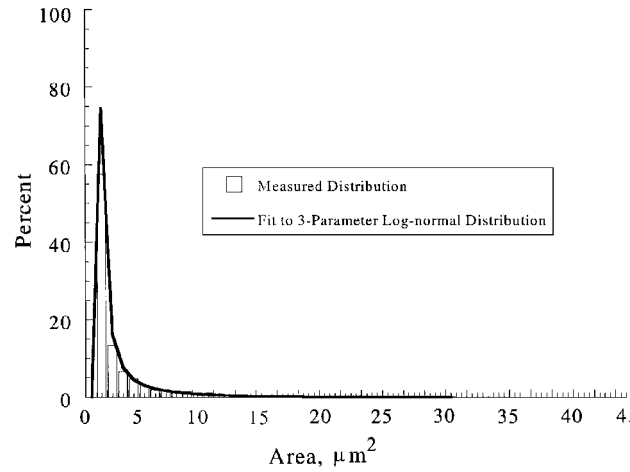

Fig. 4 Histogram of particle areas on the ST plane.

process similar to that given by Johnson et al.[23] was followed. The value of θ was iteratively selected to find the best fitting set of three parameters for the estimated density function. The log-normal parameters θ, ζ, and σ were found to be 0.191 μm^2, −0.6772, and 1.8838, respectively.

To test the normality of the logarithms of particle area, we used a Kolmogorov D test. The observed Kolmogorov D statistic was 0.0418 and resulted in a p value of <0.01. This means that the calculated set of three parameters should be rejected as the true set of three parameters for the true distribution. However, if the log-area measurements are normalized to the standard normal variate by means of[24]

$$z = \frac{\ell n(A-\theta)-\zeta}{\sigma} \qquad (2)$$

the transformed variables have a mean of 0.0000180 and a standard deviation of 0.999981. For the ideal standard normal distribution, the mean is 0.0 and standard deviation is 1.0. It is apparent that the normalized mean is nearly zero and the standard deviation is approximately 1.0. With over 1200 observations, the Kolmogorov goodness of fit test is sensitive to very slight variations from normality, especially variations in the tails of the distribution. This appears to be the case here. Because the mean and the standard deviation of the standardized variates are so close to what is expected, it is assumed that the estimated log-normal distribution explains the data adequately. Figure 4 shows the histogram of the particle distribution as well as the probability density function for the particle area. From this figure, it can be seen how well the three-parameter log-normal distribution fits the observed particle areas.

Monte Carlo Simulation

For this analysis, 1000 particles with areas above A_{th} were randomly chosen from the estimated log-normal distribution. A computer program was used to accomplish the selection process. From the observations of Lankford[10] and Newman and Edwards[15] of crack shape, each generated A_i was converted to an equivalent-area semicircular initial crack of radius r_i. Each r_i was used in the numerical crack growth model FASTRAN II to determine the fatigue life of each selected particle area. The crack growth rate data for the 7075-T6 material used in the FASTRAN II model were taken from the experimental measurements of Newman et al.[2] The data from Newman et al. were a conglomeration of results taken from the NASA group and the Chinese Aeronautical Establishment group.

To complete the Monte Carlo analysis, we compiled the 1000 generated fatigue lives to create a nonparametric CDF. With a Kolmogorov test, a degree of fit between the experimental CDF and the numerical CDF for lives was calculated to measure the effectiveness of the predictions.

Conditional Probability

As mentioned, the concept of a threshold initial area was used to bound the lower values of areas used in the numerical analysis. Because a propagating crack must already be at or above this threshold size, conditional probability calculations can be used to describe the remaining portion of the density function.

The concept of conditional probability implements relations between the probability of occurrence of events. The general formulation for conditional probability gives the probability that event X occurs given that event Y has already occurred. For the conditional probability,

$$P(X \mid Y) = \frac{P(X \cap Y)}{P(Y)} \tag{3}$$

assuming that $P(Y) \neq 0$. Creating a CDF for life to breakthrough N_b would require the calculation of the values in

$$F(N_b) = P(N_b < N) \tag{4}$$

The relationship between A_i and N_b (for a given crack shape) is one to one, and essentially A_i is inversely proportional to N_b. Because A_i and N_b are inversely proportional, the events of Eq. (4) are described as follows: event X, the probability that the initial area is greater than a given value of A; and event Y, the probability that the initial area is larger than A_{th}.

Because event X always satisfies the condition of event Y, the probability of the intersection of X and Y is equivalent to the probability of X alone, and Eqs. (3) and (4) are combined to give Eq. (5) for the CDF for area $F(A)$:

$$F(A) = \frac{P(x > A)}{P(x > A_{\text{th}})} \tag{5}$$

Conditional probability analysis in this manner allows the values of area to be chosen in any region of the particle distribution. The particles do not have to be randomly selected. In addition, this approach results in the exact CDF of fatigue life, whereas the CDF from the Monte Carlo procedure is an estimate of this CDF. Also, with the conditional approach, the tail regions can be examined more closely and sampling errors can be eliminated.

Results

Experimental Program

Each test specimen from the experimental component of this test program provided four major pieces of data: cycles to crack formation N_i, cycles to breakthrough N_b, cycles to failure N_f, and a series of plastic replicas.

A summary of N_i, N_b, and N_f for all 18 tests is given in Table 2. The shortest life to breakthrough was 36,800 cycles, and the longest finite life was 650,000 cycles. One specimen failed in the gripping mechanism of the test machine at 600,000 cycles and was treated as a runout, reducing the number of actual fatigue failures under scrutiny to 17. At 500,000 cycles, no visible cracks were observed on the specimen that failed in the grips. As for N_f, regardless of the number of cycles to breakthrough, the number of cycles beyond breakthrough necessary to reach failure averaged 6045 cycles with a standard deviation of 1144 cycles.

Table 2 Summary of cycles to crack formation N_i, breakthrough N_b, and failure, N_f

Specimen	N_i	N_b	N_f
1	70,000	108,000	115,566
2	170,000	203,000	209,711
3	16,000	50,000	55,015
4	(failed in grips)		600,000
5	100,000	143,000	147,919
6	100,000	155,000	160,795
7	1,000	72,000	77,150
8	10,000	42,000	48,272
9	35,000	90,000	93,281
10	NA	105,000	110,443
11	>425,000		650,000
12	85,000	130,000	136,170
13	7,000	52,000	58,626
14	140,000	170,000	177,400
15	85,000	120,000	127,339
16	70,000	95,000	1008,876
17	7,000	42,700	49,560
18	16,000	36,800	42,501

Crack Formation Sites

For most of the specimens, examining the replicas in reverse order under an optical microscope enabled easy identification of the nucleating defect. However, the initiation site was indiscernible for three specimens. From fractographic analysis, all the initiation sites were located, but the exact feature that initiated the crack was not evident for four specimens. The optical microscope and ESEM served as a cross reference as well as a means to classify the nucleation site if one method was indeterminate. When the combined results from the optical microscope and the ESEM images were used, 11 of the 17 critical flaws were found to nucleate at particles at or near the surface of the notch. Three cracks formed from a combined effect of either a pore and a particle or a void and a particle at or within 10–20 μm of the notch surface. The nucleation sites for the other three specimens were unable to be determined. The measured nucleating areas were converted to equivalent-area, semicircular initial cracks, which were grown to failure by FASTRAN II. The results showed that the longest experimental lives did not always correspond to the smallest initiating areas.

Figures 5–8 show ESEM images of two fracture surfaces and optical microscope digital images of the replicas from the corresponding two specimens. Figures 5 and 7 are ESEM images of the bottom fracture surface (which is contained in the ST plane) with the notch to the left-hand side of each picture. These two figures show the nucleation sites, and it can be seen that the shape of the nucleating particle is not necessarily semicircular. Figures 6 and 8 are digital images of the replica surfaces in which the ST plane is a horizontal line through the visible crack. Some of the replicas showed the crack soon after nucleation. It can be seen from these images that the cracks are propagating perpendicularly to the loading direction because the loading direction is in the vertical direction in these images. From these images, the irregular shape of the nucleating particles can be observed. The images of the replicas also show the presence of other nonnucleating particles on the notch surface.

In addition to most of the cracks initiating at inclusions, most cracks initiated in the middle 50% of thickness. One, and only one, initiation site was observed for each of the 17 finite-life specimens. The cracks were monitored with replicas to record the behavior of each crack. From these replicas, it was observed that the single nucleating crack experienced no crack interaction. All of the cracks

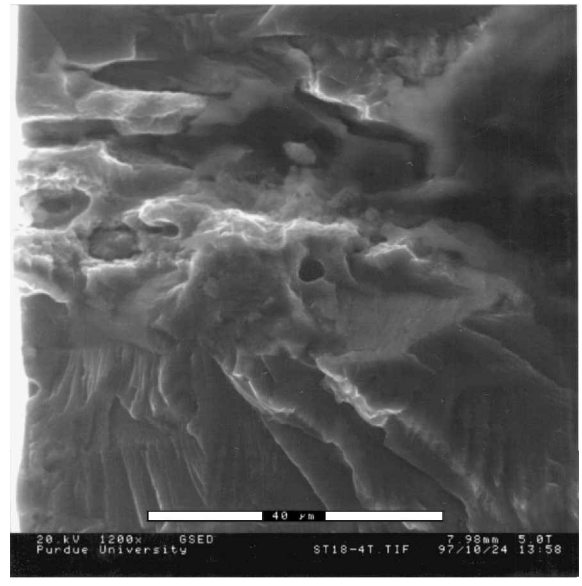

Fig. 5 ESEM image of specimen 18 fracture surface.

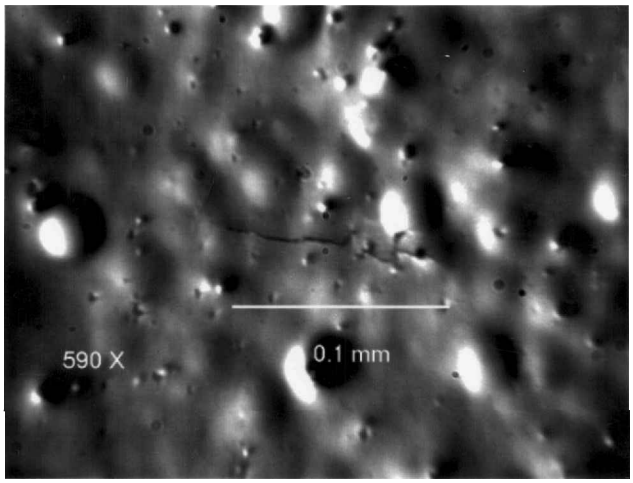

Fig. 6 Digital image of replica from specimen 18 after 16,000 cycles.

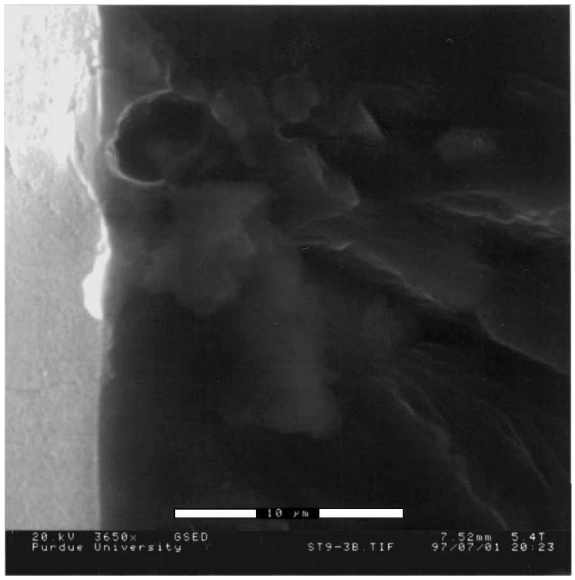

Fig. 7 ESEM image of specimen 9 fracture surface.

initiated as surface cracks, and 13 of 17 cracks initiated inside the middle 50% of the thickness. As far as position from the root of the notch, 13 out of 17 cracks initiated within ±12 deg of the root of the notch (within 94% of the maximum stress).

Threshold ΔK

From all the experimental testing, there were 18 measured fatigue lives under identical loading conditions. As mentioned earlier, one of these specimens was treated as a runout. The remaining 17 test specimens reached breakthrough at or before 650,000 cycles. Two analyses were made of the threshold behavior for the 17 finite-life specimens. For one analysis the total life was considered in which the specimen that reached breakthrough at 203,000 cycles represented the lowest applied initial ΔK resulting in finite life. The FASTRAN II results gave an initial crack size with a radius of 6.062 μm. The corresponding initial ΔK was 1.3 MPa$\sqrt{\text{m}}$, as calculated with the equations for a semicircular surface crack, and this value of ΔK was considered to be ΔK_{th} for this configuration. The results for the predicted CDFs with $\Delta K_{\text{th}} = 1.3$ MPa$\sqrt{\text{m}}$ are shown in Fig. 9. It can be seen that the predicted curve follows the experimental results quite well, and a more thorough discussion of this figure can be found in a later section. For the second analysis, only the propagation lives were used. The specimen that reached breakthrough at 203,000 cycles, with a propagation life of 71,000 cycles, represents the theoretically lowest applied initial ΔK. For the propagation life analysis, the threshold crack size was an area with a radius of 7.351 μm, corresponding to a ΔK_{th} of 1.44 MPa$\sqrt{\text{m}}$.

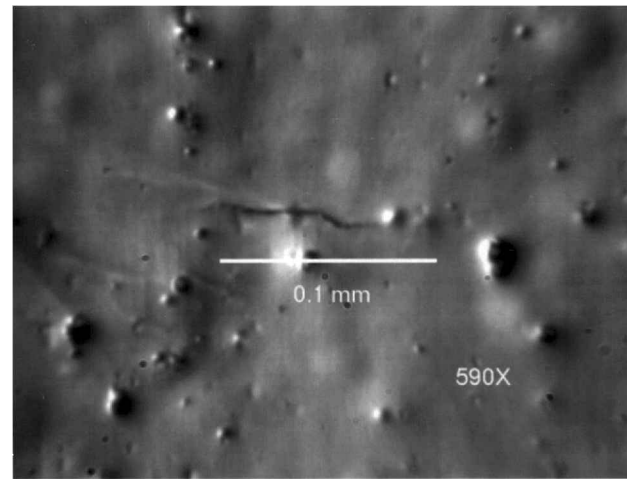

Fig. 8 Digital image of replica from specimen 9 after 16,000 cycles.

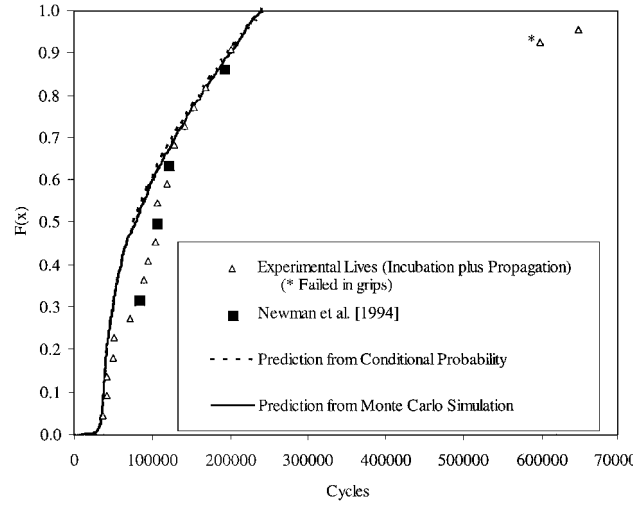

Fig. 9 Combined CDFs for cycles to breakthrough with ΔK_{th} = 1.3 MPa$\sqrt{\text{m}}$.

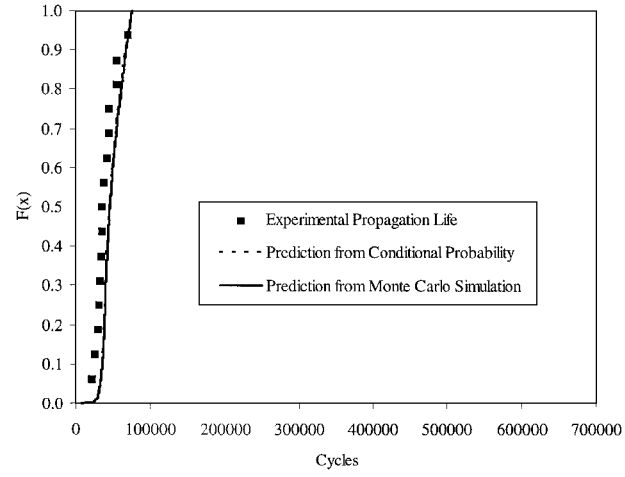

Fig. 10 CDFs for N_b based on only propagation life with ΔK_{th} = 1.44 MPa$\sqrt{\text{m}}$.

The results for the predicted CDFs with $\Delta K_{\text{th}} = 1.44$ MPa$\sqrt{\text{m}}$ are shown in Fig. 10. It can be seen that the predicted curve follows the experimental propagation lives quite well. A more thorough discussion of this figure is found in a later section.

For purposes of this investigation, the ΔK_{th} determined from the longest lifetime was based on crack propagation and did not evaluate nucleation life. In the analysis in which ΔK_{th} was determined to be 1.3 MPa$\sqrt{\text{m}}$, the failure at 650,000 cycles was treated as an

incubation-dominated lifetime. If the lifetime were adjusted for initiation life (>425,000 cycles for this specimen), the resulting life to breakthrough of 225,000 cycles would lie very close to the predicted curve of Fig. 9.

Cycles for Crack Formation

Many of the test specimens did not exhibit visible crack formation early in fatigue life. Specifically, several specimens did not develop a visible crack until after 100,000 cycles. Yet most of these test samples sustained full fatigue failure at or before 203,000 cycles. This seems to indicate that there was a significant incubation life for some of these specimens. Although the model does not incorporate an incubation period, the fatigue lives of the experimental trials are within the distribution of lives predicted by the probabilistic model. The 650,000 cycle failure is outside the range of predictions based on $\Delta K_{th} = 1.3$ MPa$\sqrt{m}$. For the six specimens that failed at or before 70,000 cycles, the average initiation life was 15% of the life to breakthrough. For the other 10 specimens for which initiation life was measured, the average initiation life was 68% of the life to breakthrough. An important result for consideration is that the specimen that failed at 650,000 cycles had a nucleation life greater than or equal to 425,000 cycles.

Probabilistic Analysis

Results from Both Numerical Techniques

In the Monte Carlo simulation, a total of 1000 particle sizes were generated from the estimated log-normal density function for the particle areas. The distribution of lives to breakthrough that resulted from the Monte Carlo simulations formed one prediction for the variability of fatigue lives. The second prediction is the distribution of lives to breakthrough from the conditional probability technique. For $\Delta K_{th} = 1.3$ and 1.44 MPa$\sqrt{m}$, the nonparametric CDF (the Monte Carlo prediction), solid curves in Figs. 9 and 10, and the parametric CDF (the conditional probability prediction), dashed curves, showed excellent agreement.

Comparison of Numerical and Experimental Results

The combined predicted and experimental results shown in Fig. 9 include four experimental data points from Newman et al.[2] In the investigation of Newman et al. of 7075-T6 aluminum, SENT specimens of dimensions nearly identical to those used in this study were tested. The four specimens tested by Newman et al. were cycled at 120 MPa and a stress ratio of 0, the same test conditions as those used in this investigation. Also, these specimens had the same stress concentration factor K_T at the notch as the specimens used in this investigation.

Figures 9 and 10 show the fatigue life to breakthrough results from both the numerical and experimental components of this investigation. One set of predicted fatigue lives, shown by the solid curve, shows the results of the Monte Carlo simulation. The second set of predicted lives, shown by the dashed curve, shows the results of the conditional probability technique. The experimental lives N_b were compiled into a nonparametric CDF by use of an $i/(N+1)$ formulation, where i is the ordered number of the data point and N is the total number of data points (all studies), in this case 21. From Fig. 9, in which $\Delta K_{th} = 1.3$ MPa$\sqrt{m}$, it is apparent that the two numerical predictions provide a good prediction of the shortest experimental fatigue lives. On the whole, the numerical predictions make conservative predictions for the experimental lives to breakthrough. As for the overall distribution of lives, the ratio of observed life to predicted life ranged from 1.01 to 1.6. From Fig. 10, in which $\Delta K_{th} =$ 1.44 MPa$\sqrt{m}$, the predictions tend to be unconservative. For this higher ΔK_{th}, the ratio of observed life to predicted life ranged from 0.63 at the shortest lifetimes to 0.91 at the longer lifetimes.

The Kolmogorov D test was utilized to compare the largest difference between the numerical CDF and the experimental CDF, in which a statistical rejection would mean that the two distributions are different at a particular level of significance. For 20 degrees of freedom, the critical D statistic is 0.45 at an α level of 0.05 and 0.55 at an α level of 0.01. For the analysis corresponding to $\Delta K_{th} =$ 1.3 MPa$\sqrt{m}$, the observed value of the D statistic for these two CDFs was 0.246. This result indicates that there is no significant evidence to suggest these two CDFs are different at either significance level. For the analysis corresponding to $\Delta K_{th} = 1.44$ MPa$\sqrt{m}$, the observed value of the D statistic for these two CDFs was 0.46. For the analysis in which a ΔK_{th} of 1.44 MPa$\sqrt{m}$ was used, the observed test statistic is larger than the critical value for $\alpha = 0.05$ and close to the critical value for $\alpha = 0.01$. These results for the CDF in which $\Delta K_{th} = 1.44$ MPa$\sqrt{m}$ indicate that the curves come from different distributions at the 0.05 level and are almost rejected at the 0.01 level also.

All of these results were made by determination a ΔK_{th} and then prediction of the CDF of fatigue lives. The value of ΔK_{th} was taken from the experimental data, and the CDF of fatigue lives was predicted by the CDF of particle areas. Laz and Hillberry[1] showed that the value of ΔK_{th} for 2024-T3 was a constant across different applied stress levels.

Discussion

Crack Nucleation from Particles

Also consistent with previous fatigue studies, most of the cracks observed in the test specimens formed at particles (11 of 17). Three of the remaining six nucleating cracks were at or near particles. These results support the findings of Newman and Edwards,[15] in which it was observed in four different alloys by different groups that the critical flaws in the sheet material nucleated at particles. This result is important information because it is one of the underlying assumptions of the probabilistic approach. The attempt to predict the variability in lifetimes is based on the variability of initial crack sizes.

Cracks Initiated from Largest Particles

For the 11 nucleation sites that could be identified as particles, the sizes of these particles (30–7200 μm^2) were from the tail of the distribution that contained the largest particles. The tail of the distribution of particle areas results in the shortest fatigue life, which is the region of greatest interest. This may suggest that an extremal distribution might be a more appropriate choice to characterize the particle areas. Additionally, if the number and the size of these largest particles in the material can be reduced, there is good reason to expect that the resistance of the material to fatigue damage may be improved.

Best Agreement in Shortest-Life Region

When Figs. 9 and 10 are examined, it is apparent that there was good agreement between predicted and experimental lives in the shortest-life region. From a design point of view, the shortest lives are the most critical. Better predictions for early fatigue failures can enable more reliable recommendations to be made for maintenance, safety schedules, and fatigue design in general. From this standpoint, the results of the probabilistic technique for the prediction of fatigue failure in 7075-T6 aluminum show a favorable degree of accuracy. For the overall distribution of lives in which $\Delta K_{th} = 1.3$ MPa$\sqrt{m}$, the ratio of observed life to predicted life ranged from 1.01 to 1.6. For the overall distribution of lives in which $\Delta K_{th} = 1.44$ MPa$\sqrt{m}$, the ratio of observed life to predicted life ranged from 0.63 to 0.91 and the predictions tended to be unconservative. From the results shown in Figs. 9 and 10, it is apparent that the effectiveness of the probabilistic model is heavily dependent on the value of ΔK_{th}, the crack growth rate characteristics of the material, and its crack nucleation behavior.

Modeling Assumptions

Most of the modeling assumptions were satisfied by the observed fatigue cracks. Cracks initiated as surface cracks, and the nominal crack propagation plane was perpendicular to the loading direction. The majority of the cracks initiated from particles in the center of the notch and in the middle of the sheet thickness. From the particle analysis the average aspect ratio was found to be 1.7, which is different from the semicircular assumption in which the aspect ratio should be 1. The shape of the initiation site and whether the initiation site is a hard particle, a debonded particle, or a cracked particle may affect the accuracy of the ΔK calculations. Although the distribution of cracked particles or debonded particles is contained in the total distribution of particles, consideration of these secondary

distributions may improve the results of future applications of the probabilistic approach.

Although most of the assumptions of the probabilistic method were satisfied for the 7075-T6, assuming a short nucleation life did not appear to be accurate for all of the specimens. One specimen, for example, showed no visible cracks before 140,000 cycles. For this specimen, the initiation life was $\sim\frac{2}{3}$ of the total life of the specimen. Many of the other specimens exhibited considerable initiation lives as well. This result was not expected, at least in reference to Newman et al.[2] and Bowles and Schijve.[25] This observation suggests that the results of this probabilistic approach might be improved if a nucleation period is considered. Currently, the approach neglected N_i but experiment showed nonnegligible N_i. Therefore future work may be improved if an incubation life is incorporated into the total life prediction.

The use of acetone has been reported to increase the fatigue life of 7075-T6.[2] In the study by Newman et al., acetone was used in the replication procedure, but in contrast to some of the results reported here, short initiation lives were observed. Although longer fatigue lives from the use of acetone have not been fully explained, one suggestion is that the acetone removes any water vapor from the crack and effectively reduces environmental attack on the crack surfaces. Proposing the reduced environmental effect would follow from the results observed by Gao et al.,[26] who found that the 7075-T651 plate showed slower crack growth rates under vacuum conditions than in humid air. However, Lankford[27] reports that the 7075-T6 sheet shows the same average rate of crack extension in humid air as under vacuum conditions. Thus it is not clear what the effect of acetone is and how it may have influenced the results in this study, if at all.

Conclusions

The major conclusions drawn from this investigation are as follows:

1) The probabilistic model closely predicted the shorter fatigue lives.

2) Cracks nucleated at particles.

3) Nucleating particles were from the large tail of the particle area distribution.

4) Cracks formed as surface cracks at the root of the notch and in the middle of the sheet thickness.

5) Nucleation was a significant portion of the total fatigue lives at the longer lives.

6) The aspect ratio of the nucleating particles may affect the initial crack driving force.

7) The value used for ΔK_{th} significantly influences the shape of the CDF.

Acknowledgment

This study was sponsored by the U.S. Air Force Office of Scientific Research under Grant F49620-93-1-0377.

References

[1]Laz, P. J., and Hillberry, B. M., "Fatigue Life Prediction from Inclusion Initiated Cracks," *International Journal of Fatigue*, Vol. 20, No. 4, 1998, pp. 263–270.

[2]Newman, J. C., Jr., Wu, X. R., Venneri, S. L., and Li, C. G., "Small-Crack Effects in High Strength Aluminum Alloys," NASA/Chinese Aeronautical Establishment Reference Publication 1309, 1994.

[3]Turnbull, A., and De Los Rios, E. R., "Predicting Fatigue Life in Commercially Pure Aluminum Using a Short Crack Growth Model," *Fatigue and Fracture of Engineering Materials and Structures*, Vol. 18, No. 12, 1995, pp. 1469–1481.

[4]Newman, J. C., Jr., "Fracture Mechanics Parameters for Small Fatigue Cracks," *Small-Crack Test Methods*, ASTM STP 1149, edited by J. Larsen and J. E. Allison, American Society for Testing and Materials, Philadelphia, PA, 1992, pp. 6–33.

[5]Turnbull, A., and De Los Rios, E. R., "The Effect of Grain Size on the Fatigue of Commercially Pure Aluminum," *Fatigue and Fracture of Engineering Materials and Structures*, Vol. 18, No. 12, 1995, pp. 1455–1467.

[6]Miller, K. J., "The Short Crack Problem," *Fatigue of Engineering Materials and Structures*, Vol. 5, No. 3, 1982, pp. 223–232.

[7]Forsyth, P. J. E., *The Physical Basis of Metal Fatigue*, Blackie, London, 1969, pp.141–152.

[8]Plumbridge, W. J., and Ryder, D. A., "The Metallography of Fatigue," *Metallurgical Review*, Vol. 14, No. 136, 1969, pp. 119–142.

[9]Pearson, S., "Initiation of Fatigue Cracks in Commercial Aluminum Alloys and the Subsequent Propagation of Very Short Cracks," *Engineering Fracture Mechanics*, Vol. 7, No. 2, 1975, pp. 235–247.

[10]Lankford, J., "The Growth of Small Fatigue Cracks in 7075-T6 Aluminum," *Fatigue of Engineering Materials and Structures*, Vol. 5, No. 3, 1982, pp. 233–248.

[11]Akiniwa, Y., Tanaka, K., and Matsui, E., "The Growth of Small Fatigue Cracks in 7075-T6 Aluminum," *Materials Science and Engineering*, Vol. A104, 1988, pp. 105–115.

[12]Navarro, A., and De Los Rios, E. R., "A Microstructurally-Short Fatigue Crack Growth Equation," *Fatigue and Fracture of Engineering Materials and Structures*, Vol. 11, No. 5, 1988, pp. 383–396.

[13]Demulsant, X., and Mendez, J., "Microstructural Effects on Small Fatigue Crack Initiation and Growth in $Ti_6A_{l4}V$ Alloys," *Fatigue and Fracture of Engineering Materials and Structures*, Vol. 18, No. 12, 1995, pp. 1483–1497.

[14]Wu, X. J., and Akid, R., "Propagation Behavior of Short Fatigue Cracks in QN Steel," *Fatigue and Fracture of Engineering Materials and Structures*, Vol. 18, No. 4, 1995, pp. 443–454.

[15]Newman, J. C., Jr., and Edwards, P. R., "Short-Crack Growth Behavior in an Aluminum Alloy—An AGARD Cooperative Test Programme," AGARD Rept. 732, 1988.

[16]Newman, J. C., Jr., "A Review of Modeling Small-Crack Behavior and Fatigue-Life Predictions for Aluminum Alloys," *Fatigue and Fracture of Engineering Materials and Structures*, Vol. 17, No. 4, 1994, pp. 429–439.

[17]Newman, J. C., Jr., "FASTRAN II: A Fatigue Crack Growth Structural Analysis Program," NASA TM 104159, 1992.

[18]Edwards, P. R., and Newman, J. C., Jr., "An AGARD Supplemental Test Programme on the Behavior of Short-Cracks Under Constant Amplitude and Aircraft Spectrum Loading," AGARD Rept. 767, 1990.

[19]Hatch, J. E. (ed.), *Aluminum: Properties and Physical Metallurgy*, American Society for Metals, Metals Park, OH, 1984, pp. 212–241.

[20]Lampman, S. R., et al. (eds.), *1990 Metals Handbook: Properties and Selection: Nonferrous Alloys and Special-Purpose Materials*, 10th ed., Vol. 2, American Society for Metals, Metals Park, OH, 1990, pp. 70–73 and 114–117.

[21]Murakami, Y., and Endo, M., "Effects of Hardness and Crack Geometries on ΔK_{th} of Small Cracks Emanating from Small Defects," *The Behavior of Short Fatigue Cracks*, edited by K. J. Miller and E. R. de los Rios, EGF Publication 1, Mechanical Engineering Publications, London, 1986, pp. 223–232.

[22]IMIX Software, Princeton Gamma-Tech, Princeton, NJ, 1993.

[23]Johnson, N. L., Kotz, S., and Balakrishnan, N., *Continuous Univariate Distributions*, Vol. 1, 2nd ed., Wiley, New York, 1994, pp. 220–222.

[24]Johnson, R. A., *Miller and Freund's Probability and Statistics for Engineers*, 5th ed., Prentice–Hall, Englewood Cliffs, NJ, 1994, p. 147.

[25]Bowles, C. Q., and Schijve, J., "The Role of Inclusions in Fatigue Crack Initiation in an Aluminum Alloy," *International Journal of Fracture*, Vol. 9, No. 2, 1973, pp. 171–179.

[26]Gao, M., Pao, P. S., and Wei, R. P., "Chemical and Metallurgical Aspects of Environmentally Assisted Fatigue Crack Growth in 7075-T651 Aluminum Alloy," *Metallurgical Transactions A*, Vol. 19A, No. 7, 1988, pp. 1739–1750.

[27]Lankford, J., "The Effect of Environment on the Growth of Small Fatigue Cracks," *Fatigue of Engineering Materials and Structures*, Vol. 6, No. 1, 1983, pp. 15–31.

A. M. Waas
Associate Editor